Physics of Fluids

RESEARCH ARTICLE | APRIL 25 2024

Breathing in danger: Mapping microplastic migration in the human respiratory system

Hafiz Hamza Riaz ; Abdul Haseeb Lodhi ; Adnan Munir ; Ming Zhao ; Umar Farooq ; M. Nafees Mumtaz Qadri ; Mohammad S. Islam

Physics of Fluids 36, 043338 (2024)
https://doi.org/10.1063/5.0205303

Physics of Fluids ARTICLE pubs.aip.org/aip/pof

Breathing in danger: Mapping microplastic migration in the human respiratory system

Cite as: Phys. Fluids **36**, 043338 (2024); doi: 10.1063/5.0205303
Submitted: 25 February 2024 · Accepted: 28 March 2024 ·
Published Online: 25 April 2024

View Online Export Citation CrossMark

Hafiz Hamza Riaz,[1] Abdul Haseeb Lodhi,[1] Adnan Munir,[1] Ming Zhao,[2] Umar Farooq,[1,3] M. Nafees Mumtaz Qadri,[1] and Mohammad S. Islam[4,a)]

AFFILIATIONS

[1]School of Mechanical and Manufacturing Engineering, National University of Sciences and Technology, H-12 Islamabad, Pakistan
[2]School of Engineering, Design and Built Environment, Western Sydney University, Penrith 2751, NSW, Australia
[3]Department of Mechanical and Computer-Aided Engineering, National Formosa University, Yunlin, Taiwan
[4]School of Mechanical and Mechatronic Engineering, University of Technology Sydney, Ultimo, NSW 2007, Australia

[a)]**Author to whom correspondence should be addressed:** mohammadsaidul.islam@uts.edu.au

ABSTRACT

The abundance of air pollutants over the last few years, including the concentration of microplastics, has become an alarming concern across the world. Initially discovered in marine life, these toxic and inflammatory particles have recently been found in human lung tissues. When inhaled, these harmful particles settle down in the lung airways and, over time, lead to respiratory failures. A recent study analyzed the microplastic transport behavior in the mouth–throat airways. However, the knowledge of the microplastic migration in bifurcating tracheobronchial airways is missing in the literature. Therefore, this first-ever study analyzes in detail the transport behavior and settling patterns of microplastic particles of different sizes and shapes at different respiratory intensities in the tracheobronchial lung airways. A numerical technique based on discrete phase modeling is employed to simulate the flow of microplastic particles in a three-dimensional realistic lung geometry. The numerical model results indicate low velocity and turbulence intensity magnitudes with smooth flow in the trachea compared to the airways of left and right lobes, which experience higher velocities and generate secondary vortices. Lower lung lobes are the deposition hotspots for the harmful microplastic particles at a lower flow rate. These hotspots shift to upper lung lobes at a higher flow rate for the same particle size. Moreover, microplastic particle size and shape influence the overall deposition rate in the tracheobronchial lung airways. The results of the current study, including microplastic accumulation regions at different breathing intensities, will contribute to the updated knowledge of pollutant inhalation and facilitate relevant treatment measures.

I. INTRODUCTION

The concerns about microplastics in the atmosphere have increased over the past decade due to the associated risks to public health and the environment. Microplastics are air pollutants, with their primary source being the industrial processing of plastic products, poor sewage systems, plastic debris, etc. (see Fig. 1). Different concentrations of these tiny particles have been detected in the oceans, soil, and atmospheric air of megacities.[1,2] The percentage of microplastics in the air is comparatively higher than in any other medium, which indicates that all humans are susceptible to inhaling such harmful particles.[3] The presence of microparticles in human lungs has been reported by multiple recent studies.[4–6] The inflammatory reactions of toxic chemicals and fibers in inhaled microplastics often lead to severe respiratory diseases. Moreover, in addition to breathing atmospheric air, individual smoking practices and invasive tracheal examinations have also been linked with microplastic exposure.[7]

The major routes for microplastic exposure to the human body include ingestion, inhalation, and dermal contact.[8] Among these routes, the concentration range of microplastics that enter the body through the inhalation of the atmospheric air is highest.[9] While many studies emphasize the presence of microplastic concentration in the human body via food[10–12] and air through the lungs,[13,14] limited studies address their transport patterns and fate in the body. Despite the small diameters of the lung airways, a high concentration of microplastics has been found in the deeper regions of the human lung.[5] The presence and deposition of such tiny harmful particles in lung airways may have an adverse impact on the respiratory system of the human body. Numerical methods like computational fluid dynamics have

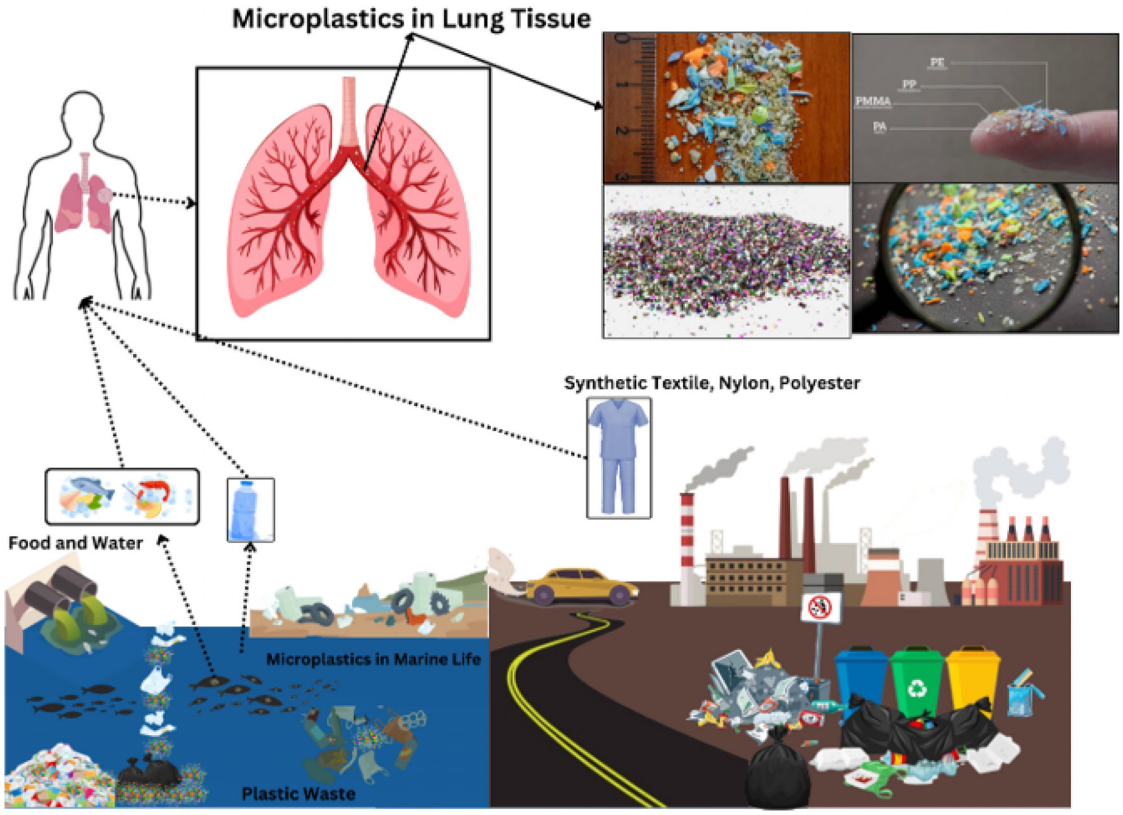

FIG. 1. Sources and migration of microplastics impacting human life.

been employed for decades by researchers to assess the transport behavior of inhaled aerosols in the human lung.[15–19] Such numerical methods can be used by experts for accurate prediction of microplastic transport and deposition in the lung airways without any danger to human life. Different human lung models have been created and employed for numerical investigations in the recent decade, including idealistic models developed by Weibel[20] and Horsfield[21] and realistic models based on CT scans. With the advancement of imaging technologies, realistic lung models have become an efficient means to study the airflow dynamics and aerosol behavior within the airways under healthy and unhealthy conditions. Multiple studies have reported particle transportation and deposition findings in different regions of the human respiratory tract, such as the nasal cavity[22–24] and upper and lower airways.[25–28] Some studies have also focused on drug delivery in the lung models of unhealthy patients, including lungs with chronic obstructive pulmonary disease,[29] stenosis,[30,31] and asthma.[32,33] Despite these, studies on the microplastic flow dynamics in the human respiratory tract are unavailable. Understanding the transport and deposition patterns of such harmful particles within human airways is essential for the accurate assessment and adequate mitigation of severe respiratory health risks. In filling this knowledge gap, Islam *et al.*[34] reported the findings on the microplastic movement and deposition in the extrathoracic region for the first time. According to the study, higher microplastic deposition in the nasal cavity was found than in the tracheal region. However, the knowledge of the transportation and deposition of microplastics in the tracheobronchial airways still needs to be added to the current literature.

The objective of the present study is to analyze the transportation and deposition of microplastics in sections of the human lung airways that have yet to be investigated previously. A computational fluid dynamics-based numerical model and a three-dimensional realistic human lung geometry are employed.

II. NUMERICAL METHODOLOGY

Numerical simulations are conducted using ANSYS-Fluent 2021 R1 to study the microplastic particles transportation and trapping within upper tracheobronchial airways. The RANS technique and the discrete phase model are employed to accurately capture airflow and microplastics flow fields.[35] The governing equations for the primary phase within the airways include:

$$\nabla \cdot (\rho \mathbf{u}) = 0, \tag{1}$$

$$\frac{\partial(\rho \mathbf{u})}{\partial t} + \nabla \cdot (\rho \mathbf{u}\mathbf{u}) = -\nabla p + \nabla \cdot (\mu \nabla \mathbf{u}) - \nabla \cdot \tau, \tag{2}$$

where ρ and μ denote the density and dynamic viscosity of the primary fluid, p is the static pressure, $\boldsymbol{u}$ is the fluid velocity, and τ represents the Reynolds stress tensor. A constant flow velocity condition at the trachea inlet is used for different air flow rates (Q), e.g., 7.5, 15, and 30 LPM corresponding to rest, light, and moderate physical activity.[36,37] A zero gauge pressure outlet condition is used at the outlet airways of

the lung model.[38] A no-slip condition for the fluid along with the trap condition is set at the rigid stationary airway walls for registering the deposited particles. The $k-\omega$ SST turbulence model is used for adequate predictions of pressure gradients near the lung walls, and the equations for the calculation of the turbulent kinetic energy and dissipation rate are as follows:

$$\frac{\partial(\rho k)}{\partial t}+\nabla\cdot(\rho\mathbf{u}k)=\nabla\cdot(\Gamma_k\nabla k)+\tilde{G}_k-Y_k, \tag{3}$$

$$\frac{\partial(\rho\omega)}{\partial t}+\nabla\cdot(\rho\mathbf{u}\omega)=\nabla\cdot(\Gamma_\omega\nabla\omega)+\tilde{G}_\omega-Y_\omega, \tag{4}$$

where Γ_k and Γ_ω is the effective diffusivity of turbulent kinetic energy (k) and dissipation rate (ω), respectively. $\tilde{G}_k$ and $\tilde{G}_\omega$ are the generation terms of turbulent kinetic energy and dissipation rate, and Y represents the dissipation. A pressure–velocity coupling scheme along with second-order discretization technique is used. The residual convergence criterion for the current study is set at 1×10^{-4}. The microplastic motion is mainly governed by drag and gravitational forces, which is expressed as follows:

$$m_p\frac{d\boldsymbol{u_p}}{dt}=\frac{1}{8}\pi\rho d_p^2C_D(\mathbf{u}-\mathbf{u_p})|\mathbf{u}-\mathbf{u_p}|+m_p\mathbf{g}, \tag{5}$$

where m_p and $\boldsymbol{u_p}$ are mass and velocity of microplastic particle, respectively. C_D is the drag coefficient, and the density of microplastic particles is set at 940 kg/m^3. The diameter of the microplastic particle is represented by d_p. Amato-Lourenço *et al.*[6] investigated and found microplastic particles in the lung tissue of 13 out of the total 20 patients under examination. They reported a size range of 1.6–5.56 μm diameter for the microplastic particles found within the airways. Therefore, multiple particle diameters for microplastics in the range of 1.6–5.56 μm have been selected, specifically 1.60, 2.92, 4.24, and 5.56 μm. The Stokes number, which is a dimensionless parameter, can be employed to describe the behavior of particles suspended in a fluid flow. This parameter represents the ratio of particle characteristic's response time to the fluid flow timescale and is determined as:

$$Stk=\frac{\rho_p d_p^2 u}{18\mu D}, \tag{6}$$

where ρ_p is the particle density and D is the diameter of the inlet surface. The Stokes number for the present study varies from 0.001 to 0.01 at 30 LPM for the given range of particle sizes.

The concept of shape factor and sphericity has been employed in the study for modeling and simulating non-spherical microplastics particles. The number of inhaled particles impacts the local deposition efficiency within the airways. Hence, after conducting the dependency study, the final number for the injected microplastic particles of each shape is selected as 30 000. All the microplastic particles of different shapes are injected at once by controlling the mass flow rate and particle number per parcel. The drag coefficient for microplastics with spherical and non-spherical shapes is calculated as follows:[39]

$$C_{D_{\text{spherical}}}=\frac{24}{Re_{sph}}, \tag{7}$$

$$C_{D_{\text{non-spherical}}}=\frac{24}{Re_{sph}}\left(1+ARe_{sph}^{B}\right)+\frac{C}{1+\frac{D}{Re_{sph}}}, \tag{8}$$

where Re_{sph} refers to the Reynolds number for particle with spherical shape and can be determined as follows:

$$Re_{sph}=\frac{\rho d_p|\mathbf{u}-\mathbf{u_p}|}{\mu}. \tag{9}$$

The Reynolds number for spherical particles ranges from 191.11 to 664.10 for different sizes at the maximum inlet flow rate of 30 LPM in the current study. The constants A, B, C, and D in Eq. (8) are dependent on the shape factor value ($\emptyset$) as

$$\mathrm{A}=\exp\left(2.3288-6.4581\emptyset+2.4486\emptyset^2\right),$$
$$\mathrm{B}=0.0964+0.5565\emptyset,$$
$$\mathrm{C}=\exp\left(4.905-13.8944\emptyset+18.4222\emptyset^2-10.2599\emptyset^3\right),$$
$$\mathrm{D}=\exp\left(1.4681+12.2584\emptyset-20.7322\emptyset^2+15.8855\emptyset^3\right).$$

The shape factor ($\emptyset$) is the ratio of the surface area of sphere (s) having the same volume as that of the particle and the actual surface area of the particle (S),[40]

$$\emptyset=\frac{s}{\mathrm{S}}. \tag{10}$$

The following is the general assumption for shape factor for different shapes of particles:
For spherical: $\emptyset=1$,
For non-spherical: $0<\emptyset<1$.

In the current study, four different shapes of microplastic particles are simulated, e.g., spherical, cube, tetrahedral, and cylindrical. The shape factor for each shape is determined using Eq. (10) and the calculated values of shape factors are listed in Table I.

A. Development of lung model and mesh generation

The three-dimensional tracheobronchial lung airways model is developed using DiCom images of a 55-year-old healthy adult. The model comprises trachea, initial generations from G1–G4, a single inlet face, and 24 outlet faces, as shown in Fig. 2(a). The unstructured mesh of lung airways with inflation layers is developed using ANSYS meshing. The number of mesh elements is selected after carrying out a grid independency study as shown in Fig. 2(b). Seven tetrahedral meshes in the range of 306 451–1 113 480 element numbers are developed, and deposition of spherical particles in the airways for each mesh is determined. The final mesh shown in Fig. 2(c), corresponding to mesh

TABLE I. Calculated shape factor values for each microplastic particle shape simulated in the current study.

Particle shape	Shape factor ($\emptyset$)
Spherical	1
Cylindrical	0.874
Cube	0.806
Tetrahedral	0.671

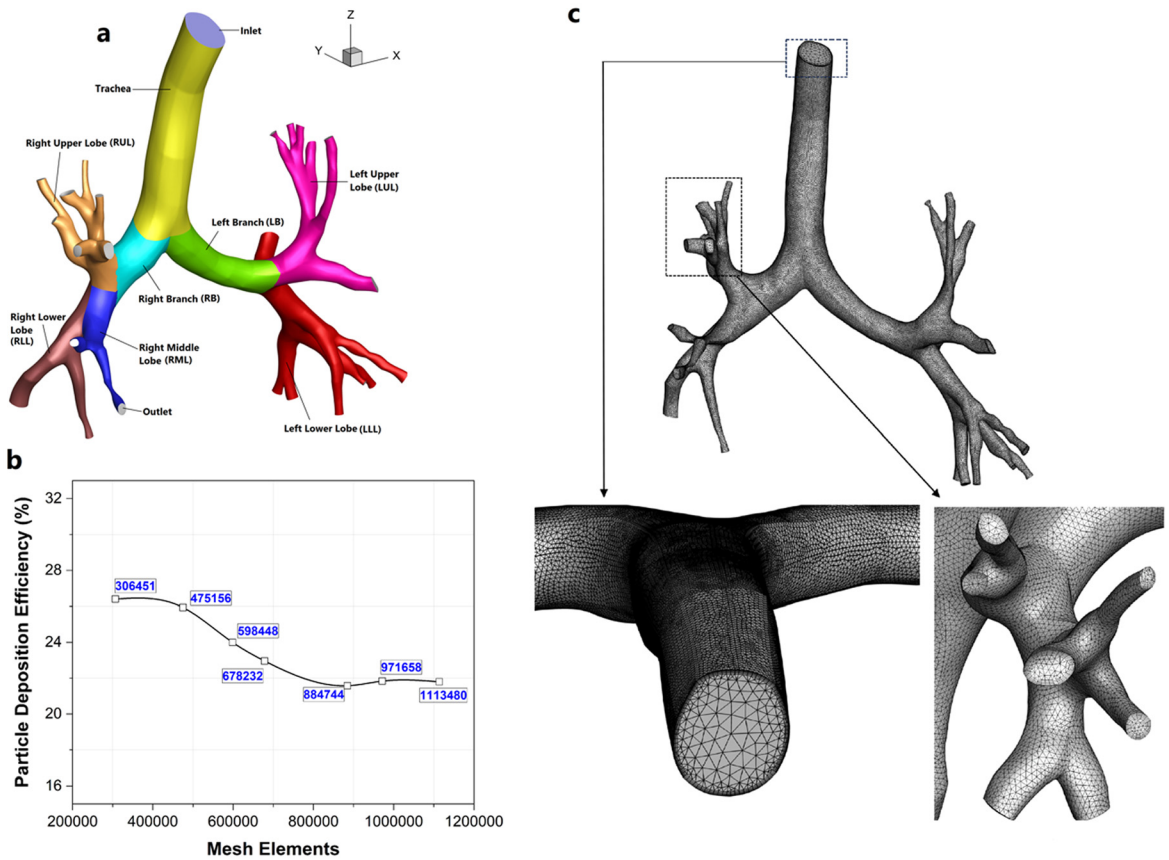

FIG. 2. (a) 3D lung airways model constructed using DiCom images of a healthy 55-year-old adult. (b) Grid independence study: comparison of deposition efficiency within airways against varying numbers of mesh elements. (c) Unstructured mesh of trachea and lung generations, inlet face at the trachea, and outlet faces of airway.

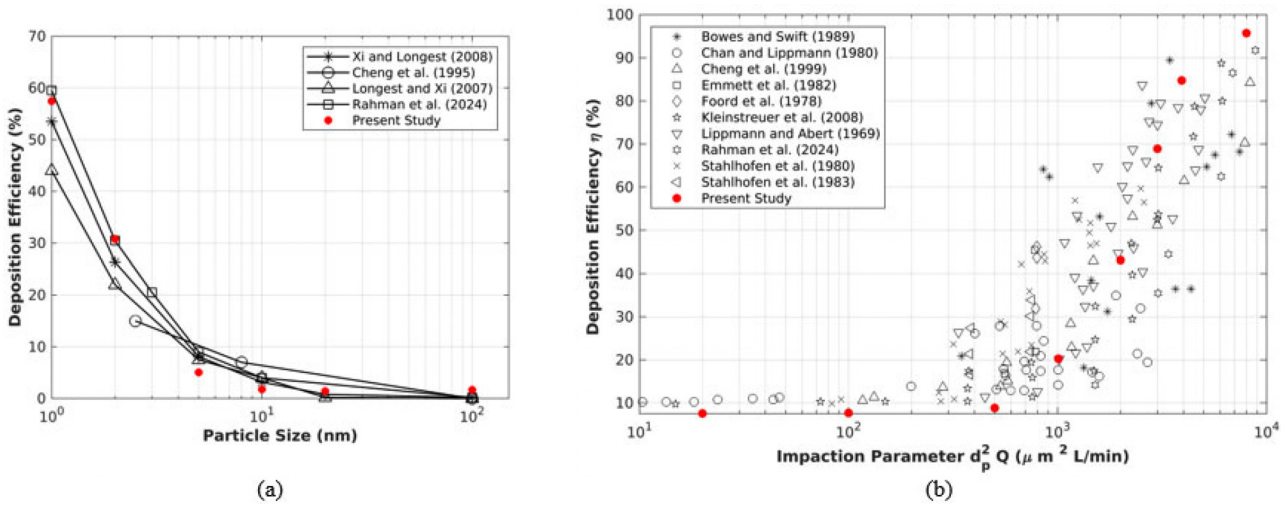

FIG. 3. Model validation: (a) comparison of deposition of nanoparticles (1 nm $\leq d_p \leq$ 100 nm) in the mouth–throat region between the present study and published research and (b) comparison of the present model of the deposition of microparticles (1 μm $\leq d_p \leq$ 20 μm) in the mouth–throat region against impaction parameter with the published research.

elements of 884 744 elements, is employed for the investigation of microplastic transport.

B. Model validation

The numerical model developed for simulating the microplastic flow and deposition within lung airways is validated using the available literature, as shown in Fig. 3. The deposition efficiency in the mouth–throat region of the respiratory tract is validated for both micro- and nano-scale particles. A comparison of deposition efficiency for different nanoparticles between the current model and literature data[17,41–43] is shown in Fig. 3(a). Similarly, in Fig. 3(b), the trend of microparticle deposition efficiency in the mouth–throat against varying impaction parameters ($d_p^2 Q$) is demonstrated for the current model and previous studies.[17,44–52] The deposition results obtained from the present model illustrate a similar trend as reported in the available literature.

III. RESULTS AND DISCUSSION

A. Flow characteristics

The influence of the respiratory intensity on the flow profile is analyzed using three different inlet air flow rates of 7.5, 15, and 30 LPM. The velocity streamlines at these air flow rates are shown in Fig. 4, in which clear differences in the generation of vortices can be found between different inlet air flow rates. A high inlet flow rate leads to the maximum generation of vortices starting from the first bifurcation of the tracheobronchial tree and down to the last bifurcation of

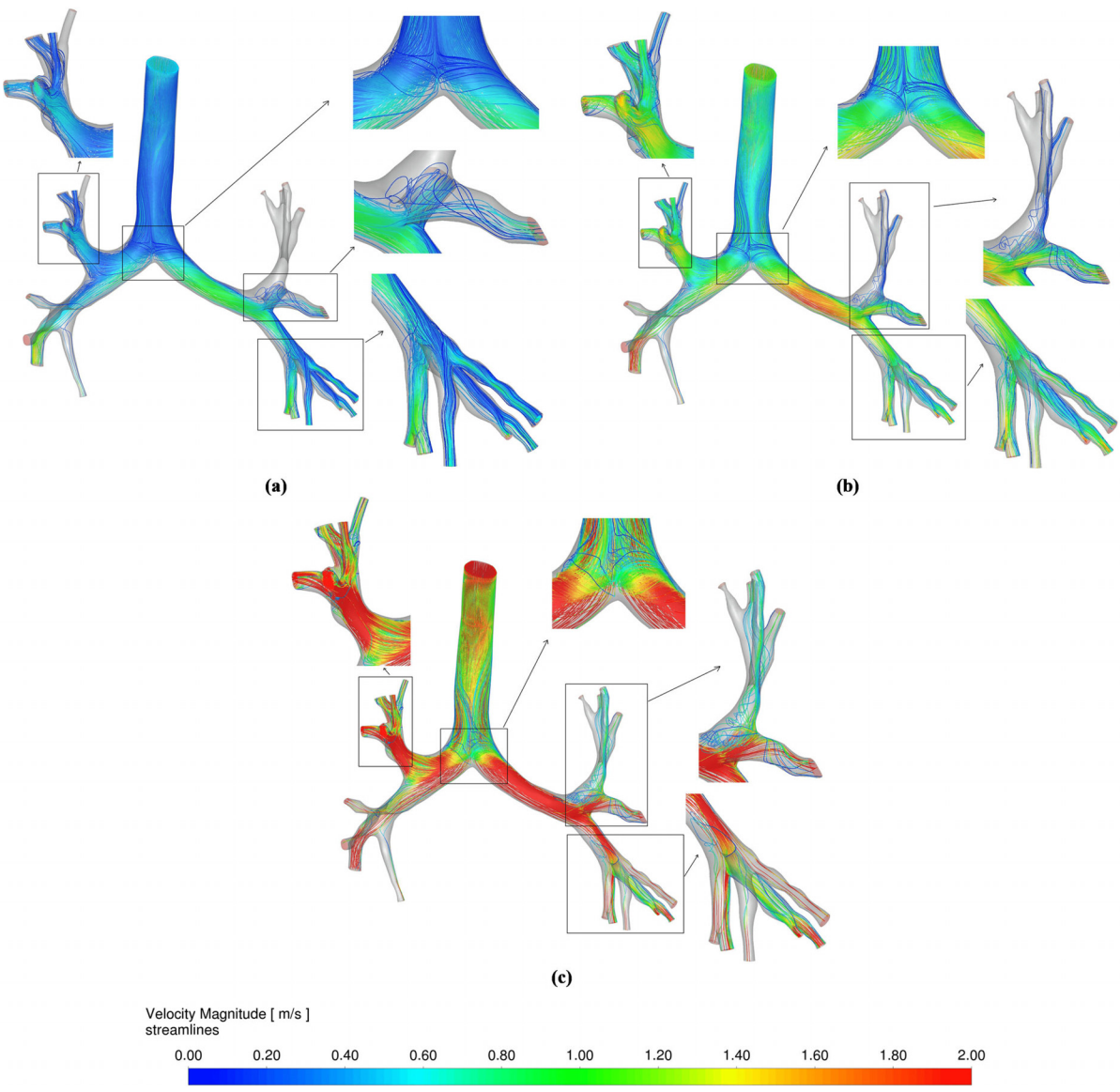

FIG. 4. Flow velocity streamlines in the tracheobronchial lung airways for air flow rates of (a) 7.5, (b) 15, and (c) 30 LPM.

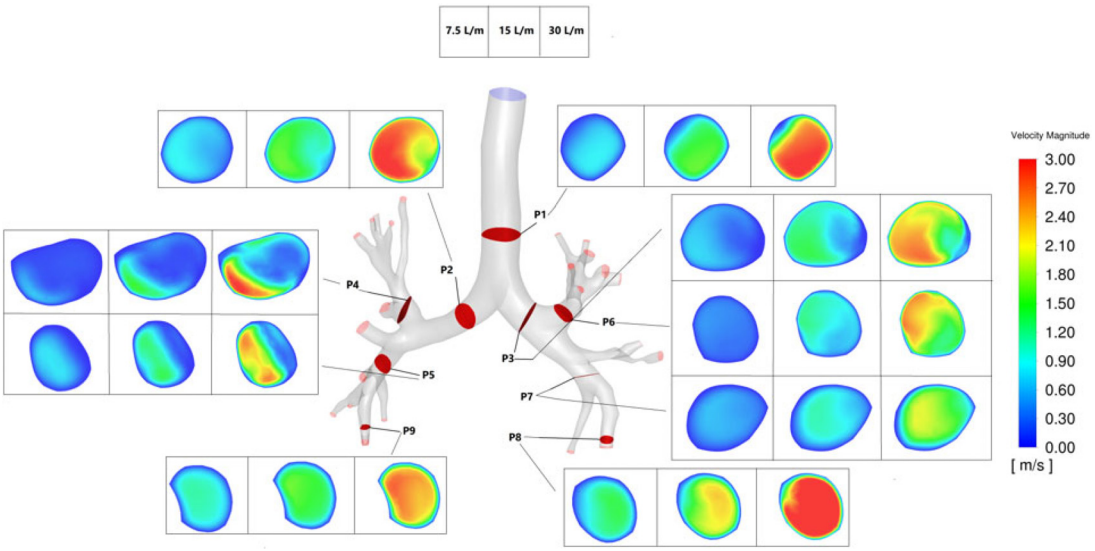

FIG. 5. Velocity contours at different cross-sectional planes (P) and air flow rates within tracheobronchial airways.

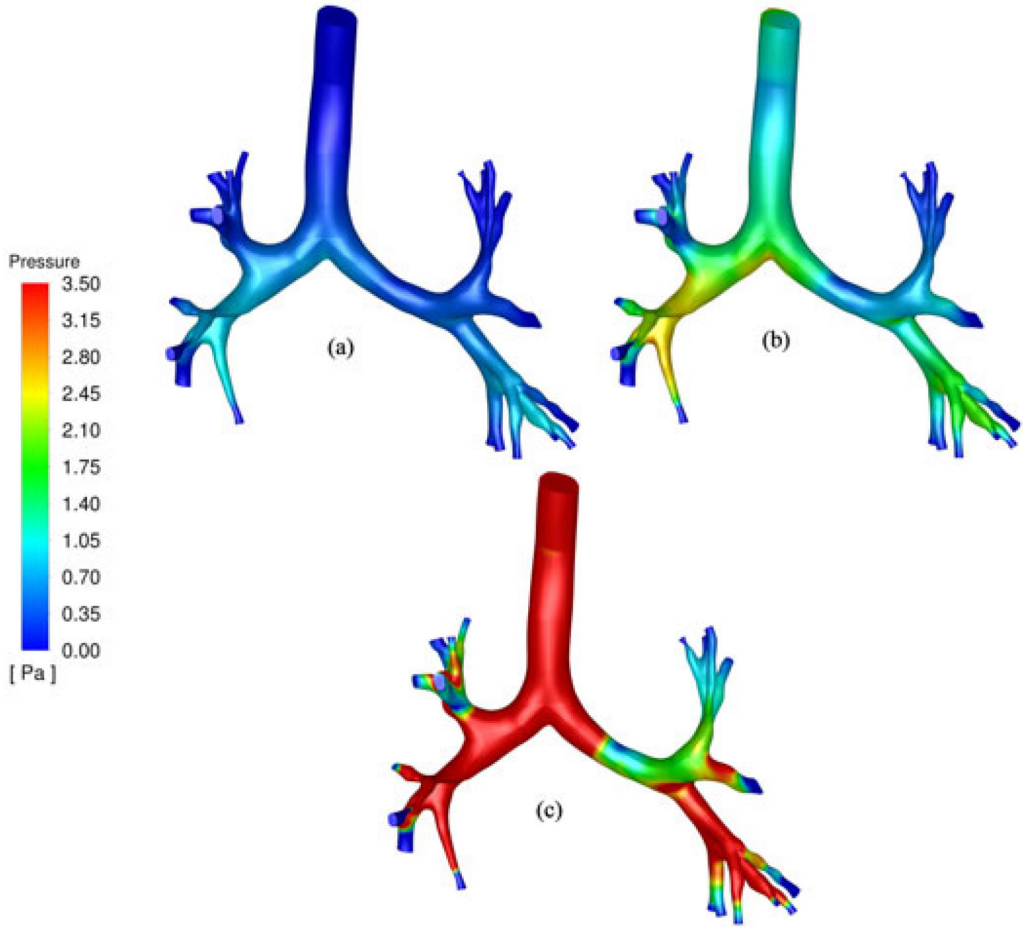

FIG. 6. Pressure distribution in the tracheobronchial lung airways for air flow rates of (a) 7.5, (b) 15, and (c) 30 LPM.

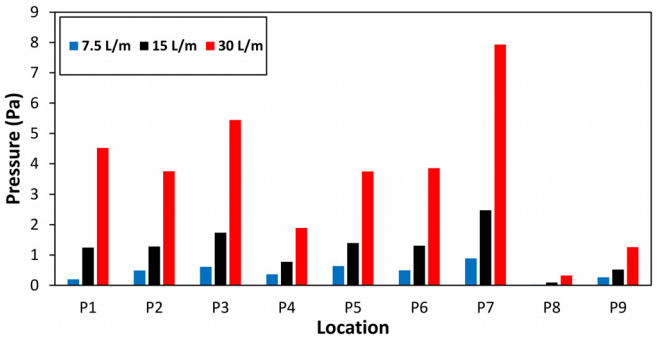

FIG. 7. Pressure distribution at different planes along the tracheobronchial lung model (see Fig. 5 for planes location).

the lung model under study. While the left upper lobe shows negligible velocity streamlines for a low flow rate, the same region experiences high secondary vortices for a flow rate of 30 LPM. The trachea, being larger in size, has the lowest velocity as compared to the generations that follow. The narrow airway in the left branch of the lung experiences high-velocity magnitude (see plane 2 and plane 3 in Fig. 5) whereas the peak velocity is generated in the right lower lobe. At an elevated flow rate of 30 LPM, maximum velocities are also found in the right upper lobe. Figure 5 illustrates the velocity contours at different planes covering each lobe along the lung model at multiple inlet air flow rates. The airways of the right and left lower lobes, being the smallest in size, show significant magnitudes of velocity at each inlet flow rate. Moreover, a considerable flow inclination toward the inner walls is found near the bifurcation points, including plane 3, plane 4, and plane 6. This phenomenon is more prominent for higher air flow rates due to the generation of flow vortices.

The variations in the inlet flow rate significantly disrupt the pressure distribution within lung airways, as demonstrated in Fig. 6. The larger sections of the lung, e.g., trachea, right branch, right middle lobe, right lower lobe, and left lower lobe, experience higher pressure values and resistance to the incoming airflow. The sudden curvatures in the airways, accompanied by nonuniform airway sizes, affect the pressure magnitudes. The pressure values at different planes in Fig. 7 show a direct relation between the respiratory intensity and generated

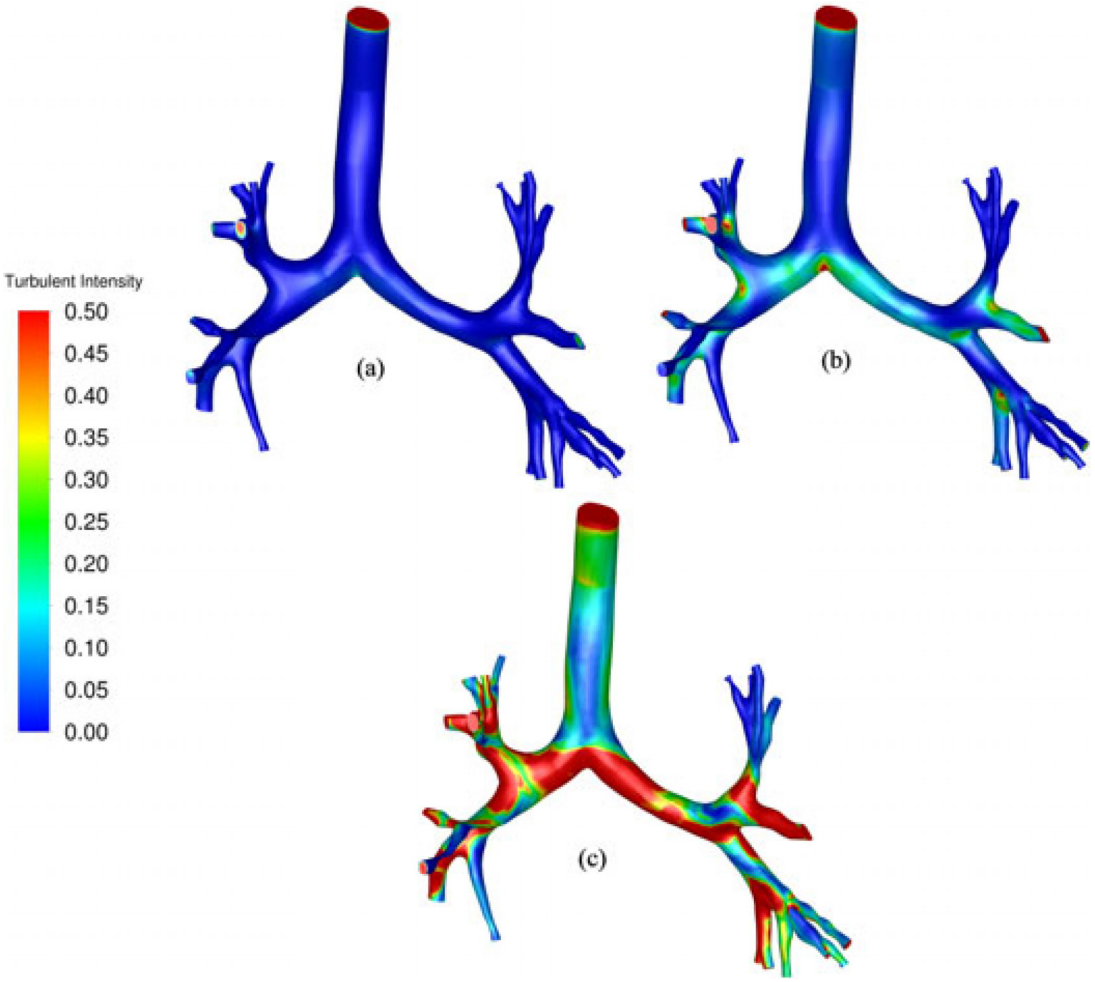

FIG. 8. Turbulent Intensity in the tracheobronchial lung airways for air flow rates of (a) 7.5, (b) 15, and (c) 30 LPM.

pressure at all locations within tracheobronchial lung airways. The pressure loss across other planes can be attributed to the complexity of the airway structure and wall frictions. The continuous series of expansions and contractions in the airway tree results in increasing and decreasing pressure values across the lung airways. Near all outlets, pressure drops to zero (plane 8 and plane 9), satisfying the boundary condition and the overall pressure drop, which drives the flow. In addition to this, the pressure drops more intensely at a higher flow rate because of significant flow velocity and friction between the lung walls.

Figure 8 shows the turbulence intensity contours for the air flow rates of 7.5, 15, and 30 LPM. Turbulence intensity, a ratio of fluctuations in the flow velocity to the average flow velocity, is an adequate parameter to indicate the flow turbulence. Significantly higher turbulence levels are found for the 30 LPM flow rate, as the more significant flow rate causes high chaotic flows within the intricate network of non-uniform airways (see Fig. 4). High turbulence intensity at bifurcation points is found for the trachea and each lobe at air flow rates of 15 and 30 LPM. At lower air flow rates, the velocity distribution is relatively smooth and less chaotic to cause any considerable turbulence in the flow. Such variations in the turbulence intensity at different air flow rates will ultimately influence the microplastic transportation and deposition within the lung airways.

B. Microplastic deposition

The overall deposition efficiencies of microplastic particles of different shapes and diameters in the lung airways are shown in Fig. 9(a). The microplastic sizes simulated in the current study include 1.60, 2.92, 4.24, and 5.56 μm. At 7.5 LPM, minimum deposition efficiency is found for each microplastic particle shape and size compared to the higher air flow rates. At a lower flow rate, the spherical particle has the lowest deposition rate, whereas tetrahedral and cylindrical particles tend to trap more within the lung airways. This pattern changes at 15 LPM, where spherical particles show similar or higher deposition efficiencies than tetrahedral particles, especially for large particle sizes. At 30 LPM, the cube, tetrahedral, and cylindrical particles dominate the deposition efficiency values for particle sizes of 4.24 and 5.56 μm. Although the non-spherical particles have similar deposition efficiency ranges, they demonstrate random deposition trends with peak deposition values alternating between cube, cylindrical, and tetrahedral particles at different sizes and air flow rates. However, increasing the flow rate impacts the deposition of spherical particles in a manner such that smaller particle sizes of 1.60 and 2.92 μm deposit more, whereas larger particle sizes deposit less than non-spherical particles. The overall trend shows higher microplastic deposition within tracheobronchial lung airways at higher air flow rates. The maximum deposition efficiency for all microplastic particles of size 5.56 μm is 3.80%, 5.10%, and 5.81% for 7.5, 15, and 30 LPM, respectively, as shown in Fig. 9(b). This can be explained in terms of flow disturbances and vortices generations at higher air flow rates, which causes the inhaled microplastics to diverge from the primary flow path and collide with the nearby lung wall. The opposite happens at lower air flow rates, where the

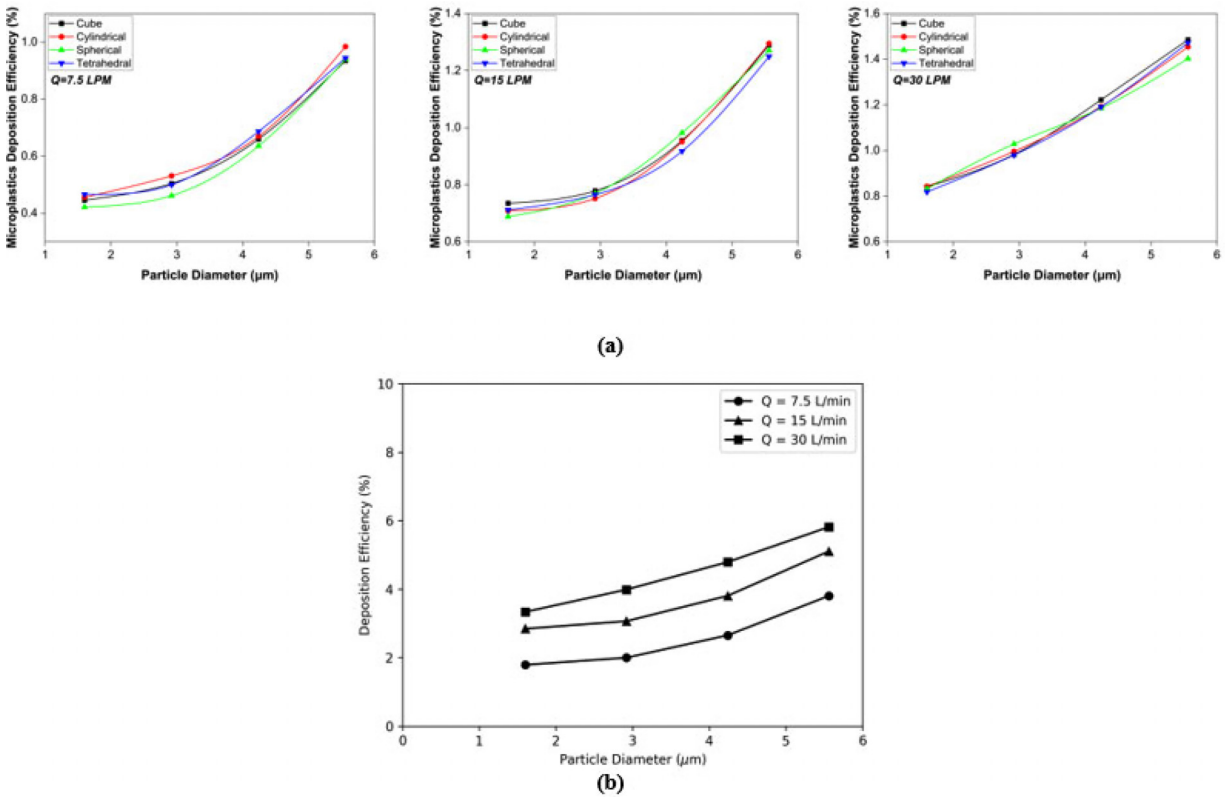

FIG. 9. (a) Deposition of different microplastic shapes for the flow rate of 7.5, 15, and 30 LPM and (b) total deposition efficiency of all microplastic shape at different air flow rates and particle size.

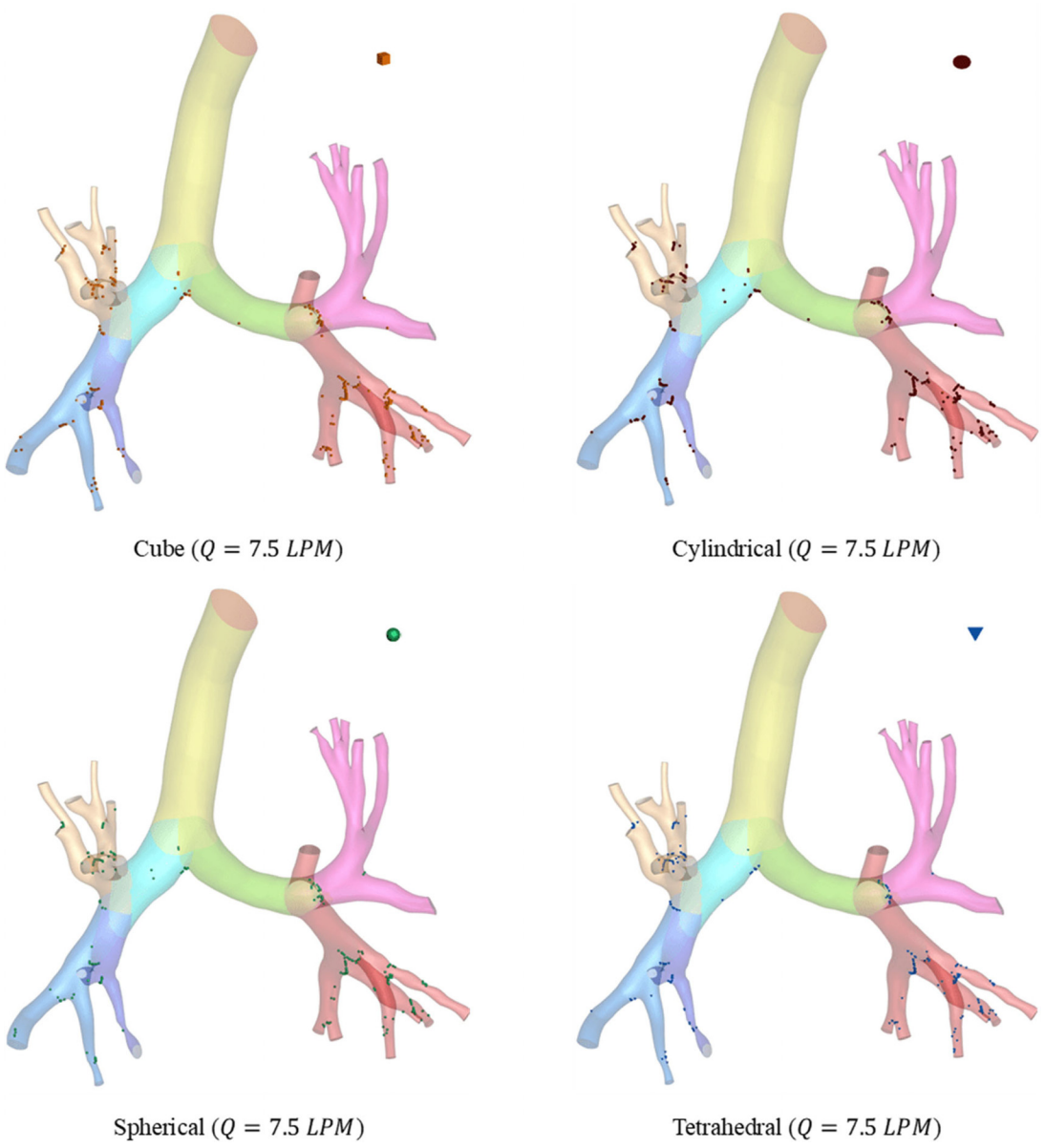

FIG. 10. Local deposition of microplastics in the tracheobronchial lung airways for different shapes at the flow rate of 7.5 LPM and 1.6 μm diameter size.

microplastic particles have enough time to align their path trajectories according to the airflow and move into the deeper lung airways.

Figure 10 visualizes the microplastics distribution within the tracheobronchial lung airways for 7.5 LPM and 1.60 μm particle size. A negligible number of microplastic particles are deposited in some areas of the lung such as the trachea, left upper lobe, and left branch. At this lower flow rate, the inertial impaction of inhaled microplastics is not strong enough to deviate and make them collide with the lung walls. Moreover, the small particle size also does not contribute much to the deposition rate of microplastics. The low incoming flow rate combined with small particle size results in a small Stokes number, which defines the reaction time for the particle to any changes in the fluid flow. A small Stokes number indicates that microplastic particles can quickly adjust their trajectories according to the fluid flow as the air moves from the trachea to the deeper airways. Hence, only a few particles tend to deposit at the bifurcation points of each lung region at 7.5 LPM as shown in Fig. 10. Moreover, when compared with other lung regions, the airways of the left lower lobe receive a high deposited particle count. At the high flow rate of 30 LPM, an increased deposition rate is found, as shown in Fig. 11, for each microplastic particle shape. Here, a high Stokes number due to the high flow rate and large diameter size of 5.56 μm limits particles from aligning their flow directions

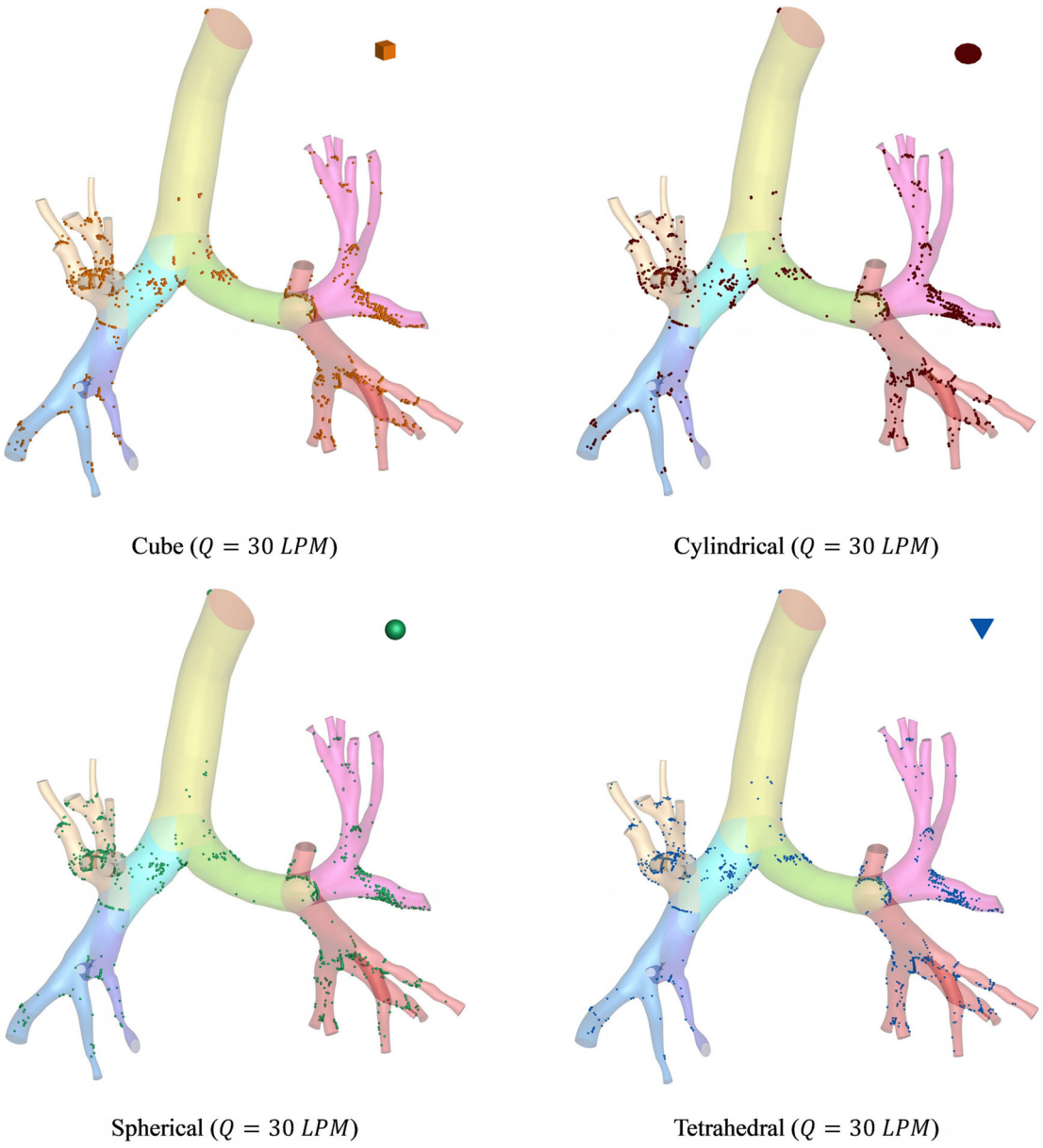

FIG. 11. Local deposition of microplastics in the tracheobronchial lung airways for different shapes at the flow rate of 30 LPM and 5.56 μm diameter size.

with the changing airflow paths at the sharp curvatures present within the airway tree. The regions where particles do not deposit at a lower flow rate receive considerable deposited particle count at 30 LPM, including the left branch and left upper lobe.

The majority of the microplastic particles of each shape deposit and accumulate near bifurcation regions instead of spreading all over the airways evenly. This can better be visualized through the accretion contours in Fig. 12, which shows the lung regions where inhaled microplastics are inclined to deposit more and form particle clusters. For 1.6 μm particle size, negligible microplastic particle clusters are formed in the tracheobronchial lung airways despite lower or higher inhalation flow rate. For 2.92 μm particle size, cluster formation in the left lung is found. These particle clusters enhance at the flow rate of 30 LPM, especially in the left lower lobe. For the inhaled microplastic particle size of 4.24 μm, cluster formation initiates even from the lower flow rate of 7.5 LPM and increases continuously as the respiratory intensity enhances. Significant clusters in the right branch, left upper lobe, and left lower lobe are found for this particle size. For the large particle size of 5.56 μm, at 7.5 LPM, microplastic particles accumulate dominantly in the left and right branches of the lung. However, as the inlet flow increases to 15 LPM and eventually to 30 LPM, the profile of the cluster formation moves from the left and right branches to the

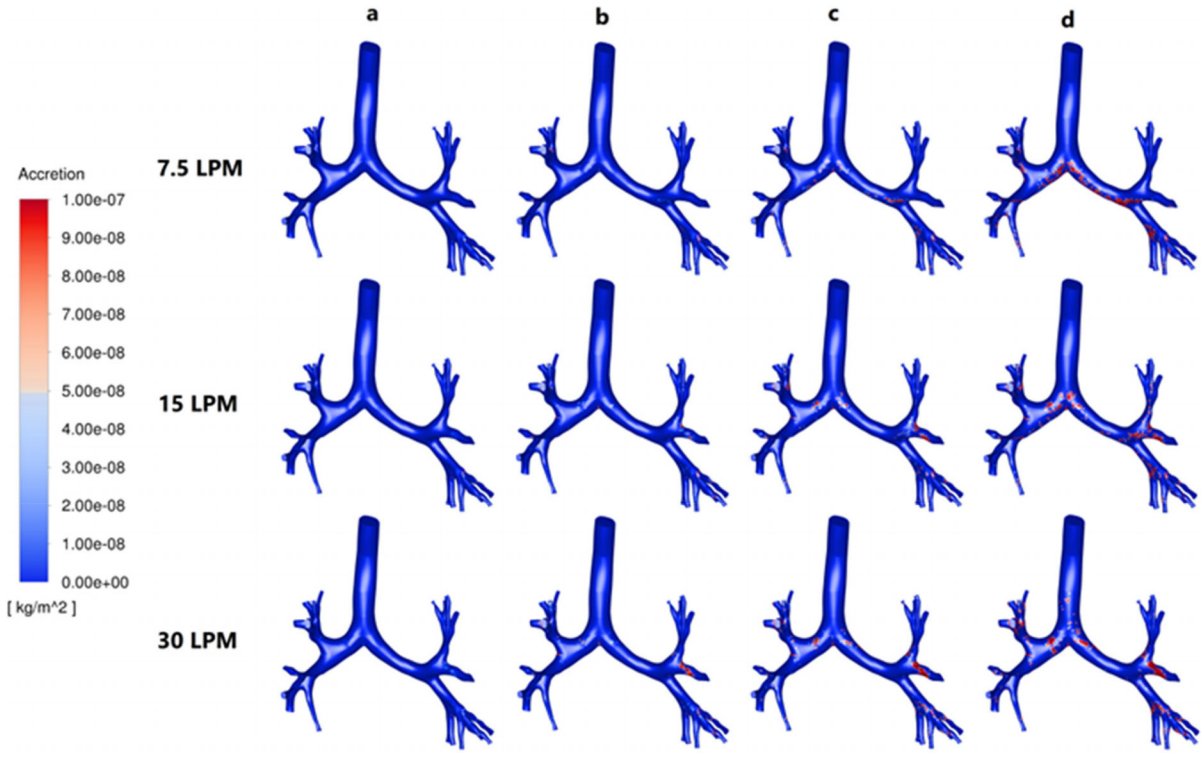

FIG. 12. Accretion contours for microplastics deposition at different air flow rates and particle sizes of (a) 1.60, (b) 2.92, (c) 4.24, and (d) 5.56 μm.

trachea and side lobes. At 30 LPM, lung regions, including the trachea, left upper lobe, left lower lobe, and right upper lobe, contain the maximum number of accumulated 5.56 μm microplastic particles.

The region-wise deposition plots shown in Fig. 13 give a better picture of the trend of microplastic particles trapping at different air flow rates and sizes. For 7.5 LPM, particles of sizes 1.60 and 2.92 μm get trapped evenly between the trachea, RB, RL, LUL, RML, and RLL. At the same time, large particles of 4.24 and 5.56 μm deposit early and largely at RB, LB, and RUL because of the high Stokes number for large particles at a constant flow rate. The maximum number of deposited particles for this flow rate is at LLL. When the flow rate increases to 15 LPM, RUL becomes the dominant region for microplastic deposition, followed by LLL. Further increasing the flow rate to 30 LPM keeps the deposition efficiency values the same for all lung regions except LUL, which experiences slightly higher particle collisions compared to lower air flow rates. The primary reason behind higher deposition efficiency values for certain areas like LLL for each flow rate along with RUL, LUL at 15 LPM and 30 LPM is the high turbulence intensity and chaotic flow regions at these sites (see Figs. 4 and 8). Other regions, including trachea, LB, RB, RML, and RLL, experience comparatively less chaotic flows and eventually less particle deposition at each flow rate.

A more detailed and quantitative analysis of the microplastic deposition for each particle shape within lung airways using MATLAB-generated plots is shown in Fig. 14. The deposition concentration of microplastic particles with cube, cylindrical, spherical, and tetrahedral shapes and 5.56 μm diameter along the vertical length of the tracheobronchial lung airways is plotted for 7.5 LPM and 15 LPM. An approximately similar trend with minimal deviations between the deposition curves of each particle shape is found. At 7.5 LPM in Fig. 14(a), the hotspots for the microplastic deposition are mainly the lower lobes of the lung, including the right middle lobe, right lower lobe, and left lower lobe, specifically from $z = -0.13$ to $z = -0.18$ m. Both upper lobes of the left and right lungs, along with the tracheal pipe, experience low microplastic particle collisions at a lower flow rate. These regions exist between the length of $z = -0.02$ to $z = -0.12$ m. As the flow rate increases to 15 LPM, a shift in the deposition hotspots is found. At the high flow rate, as shown in Fig. 14(b), maximum deposition of the inhaled microplastics is found in the upper lobes of the lung, especially in the right upper lobe and lower section of the trachea from regions between $z = -0.08$ and $z = -0.11$ m. The total deposition efficiency of microplastics in the upper lobes (right upper lobe and left upper lobe), lower lobes (right middle lobe, right lower lobe, and left lower lobe), and trachea is 0.57%, 2.24%, and 0.02%, respectively at 7.5 LPM. These deposition values change to 2.70%, 1.93%, and 0.11% in the upper lobes, lower lobes, and trachea, respectively, at 15 LPM. The smooth airflow and low turbulence, even at a larger flow rate in the trachea, reduce particle deposition in this region. The lower section near the bifurcation experiences considerable microplastic deposition at a high flow rate due to the flow splitting and generation of secondary vortices. Furthermore, the reason for the high microplastic particles trapping in the upper lobes for higher flow rate includes high inertial impaction, which leads to particles colliding at the lung walls whenever any obstructions in the form of bifurcating point and curvature occur

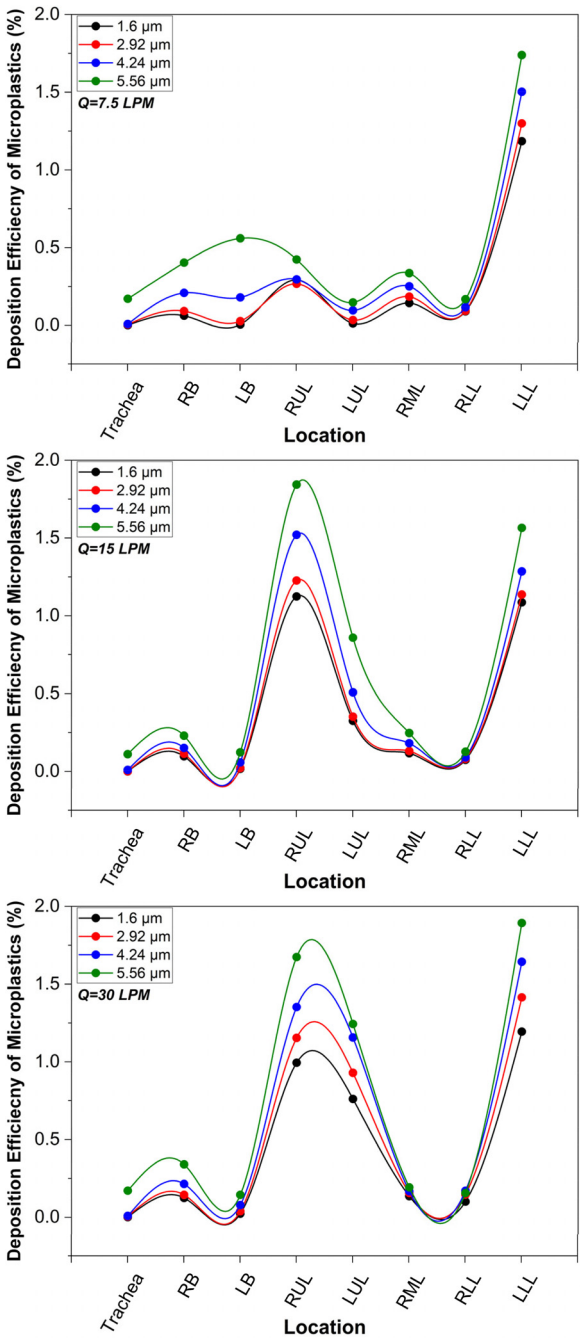

FIG. 13. Microplastic deposition at different regions of the lung: trachea, right branch (RB), left branch (LB), right upper lobe (RUL), left upper lobe (LUL), right middle lobe (RML), right lower lobe (RLL), and left lower lobe (LLL).

within their pathway. This phenomenon is avoided at lower air flow rates where particles have adequate response time to adjust their paths without much flow disruptions and collisions at the walls of upper lung lobes and can move and deposit in the lower airways.

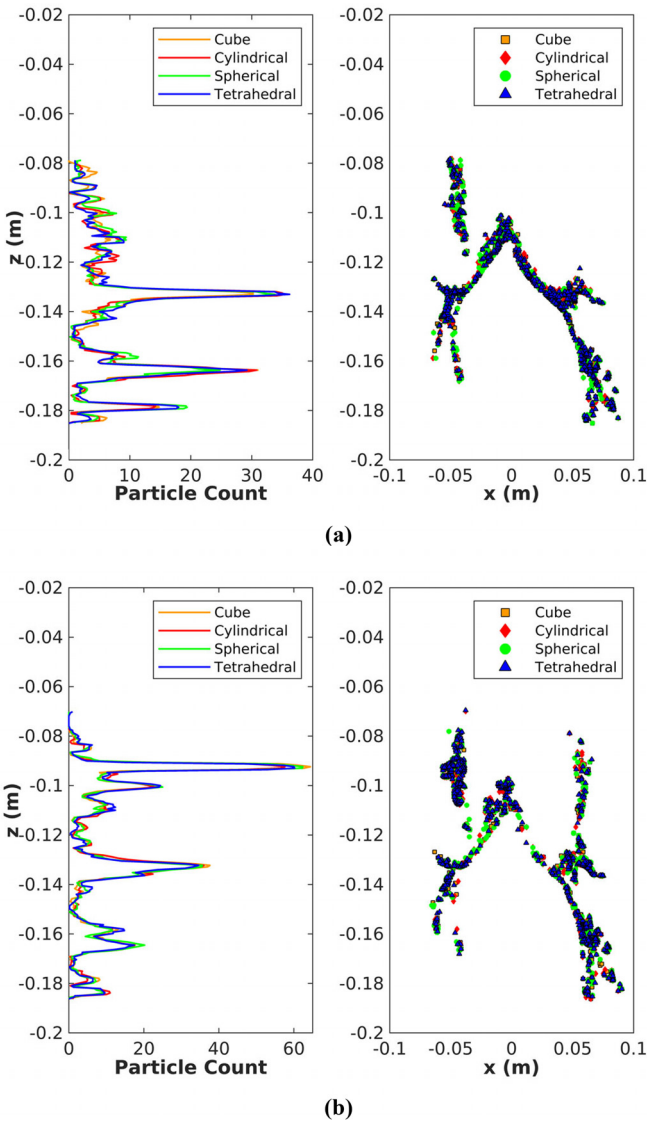

FIG. 14. 5.56 μm deposited microplastics distribution along the tracheobronchial lung airways at (a) 7.5 and (b) 15 LPM.

The microplastic deposition hotspots in the lung airways for different particle sizes at 30 LPM are demonstrated in Fig. 15. Unlike air flow rates, similar deposition hotspots are found for each microplastic particle size ranging between 1.60 and 5.56 μm diameter. These deposition hotspots are mainly the bifurcation sections across the different lung regions of the right and left lungs. The concentration of microplastics at these deposition hotspots increases continuously as the particle size is enhanced. This is because small-sized particles can conveniently find their way through the upper tracheobronchial lung airways, whereas the large particles are prone to deviate and deposit in the earlier airways because of strong inertial impaction. A significant increase in the particle count at the hotspots is found for the 5.56 μm particle size, as shown in Fig. 15(d). A considerable number of 5.56 μm

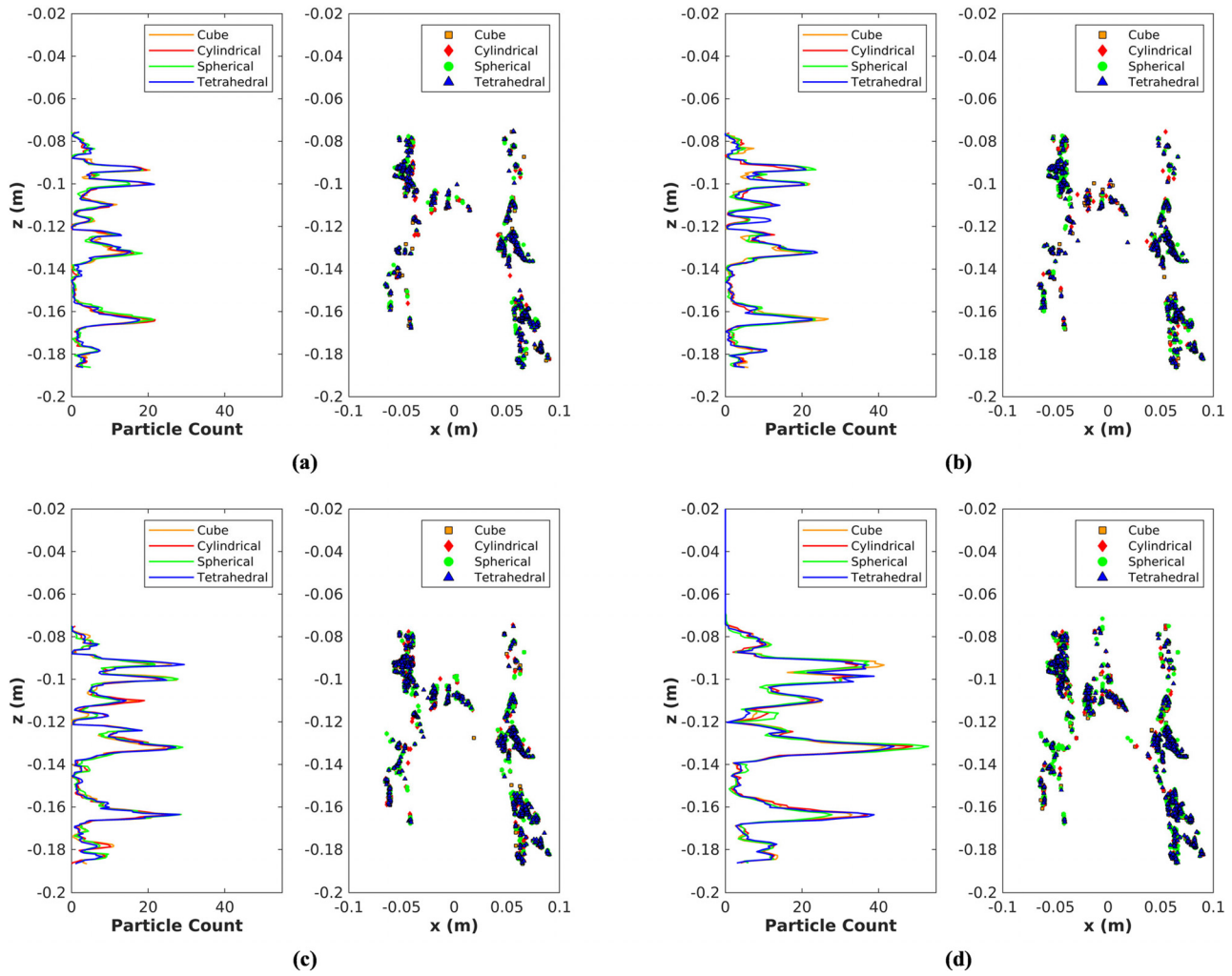

FIG. 15. Deposited microplastics distribution along the tracheobronchial lung airways at 30 LPM for particle size: (a) 1.60, (b) 2.92, (c) 4.24, and (d) 5.56 μm.

size microplastics deposit in the trachea from $z = -0.08$ to $z = -0.1$ m than the lower particle sizes. Moreover, for non-spherical harmful particles, including cube, cylindrical, and tetrahedral, higher deposition efficiencies at almost each deposition hotspot are found than spherical particles. This is due to the asymmetric particle shape and altered aerodynamic properties like enhanced surface drag, which further increases their penetration probability in the lung airways compared to the spherical particle. This increase is more prominent for upper lung lobes in the region between $z = -0.08$ and $z = -0.12$ m.

IV. CONCLUSION

Microplastic particles have been found lodged within human lung tissues for the very first time recently. Continual exposure to these harmful particles disrupts the biophysical functions of the pulmonary system and induces severe respiratory diseases. The experts emphasize the prevalence of microplastic pollution on a global scale, making its human exposure unavoidable. A detailed investigation of microplastic transportation and accumulation within the human lung is critical for understanding their flow patterns and updating associated health risk assessments. The current study investigates the inhalation of microplastic particles at different respiratory intensities and particle sizes. The deposition hotspots of microplastics within lung airways, as well as flow patterns for different inhalation flow rates, are analyzed as well. The following are key findings:

- The tracheal pipe has low-velocity distributions at each flow rate compared to the airways that follow. Whereas narrow airways of the right lower lobe have maximum magnitudes of flow velocities, especially at 30 LPM. As the flow rate increases, the generation of secondary vortices intensifies, and these vortices are highly region-specific. At a large inhalation flow rate, lung lobes, especially the left upper lobe and left lower lobe, experience a higher generation of secondary vortices than the right lobes due to highly complicated airway structure. High turbulence intensity magnitudes are found at 30 LPM for the left upper and lower

lobes along with the right upper lobe due to the chaotic airflow within the corresponding airways.
- The inhalation intensity of microplastic particles directly controls their deposition rate. A total of 3.80%, 5.10%, and 5.81% microplastics are deposited at 7.5, 15, and 30 LPM, respectively in the tracheobronchial airways for particle size of 5.56 μm. The microplastics deposition hotspots also vary with the increasing inhalation flow rate.
- Microplastic deposition is negligible for lung regions like left and right upper lobes at a lower flow rate irrespective of the particle size and shape due to low inertial impaction. The total microplastic deposition at 7.5 LPM is 0.57% in the upper lobes and 2.24% in the lower lobes. At this flow rate, particles with low Stokes numbers have enough reaction time to align their trajectories without many collisions in the upper lobes and move deeper into the airways in the lower lobes. Whereas at 15 LPM, upper lobes deposition rises to 2.91% while lower lobes drop to 1.93%. The high turbulence intensities lead to significant microplastic deposition in the left and right upper lobes at larger air flow rates.
- The trachea, having a comparatively less complicated airway structure, experiences smooth air and particle flow without considerable disturbances. The maximum microplastic deposition found here is 0.17% at 30 LPM, which is still lower than any other lung region. Moreover, particles deposit only at the lower section of the trachea due to the splitting of the flow and generation of secondary vortices at the first bifurcation.
- The shape and size of the microplastic particles impact the deposition efficiency in the tracheobronchial lung airways. As compared to the spherical particles, the varied shape factor and aerodynamic drag acting on the non-spherical particles enhance their deposition rate, especially at the hotspots for smaller particle sizes of 1.60, 2.92, and 4.24 μm.

The findings on the size and region-specific microplastic deposition in the tracheobronchial lung airways could facilitate the assessment of health risks associated with inhaling excessive toxic pollutant particles. However, extended investigations on the microplastic flow in the respiratory tract could be helpful for enhanced understanding. Future studies would include using a complete lung model including mouth–throat, nasal cavity, trachea, and upper and lower airways up to 23rd generation. Furthermore, the impact of respiratory diseases, as well as environmental factors, will also be considered.

AUTHOR DECLARATIONS

Conflict of Interest

The authors have no conflicts to disclose.

Ethics Approval

This study was approved by the Prince Charles Hospital Human Research Ethics Committee (Approval No. HREC/16/QPCH/276) and the Queensland University of Technology Human Research Committee (Approval No. 1600000923).

Author Contributions

Hafiz Hamza Riaz: Data curation (equal); Formal analysis (equal); Investigation (equal); Methodology (equal); Writing – original draft (equal). **Abdul Haseeb Lodhi:** Data curation (equal); Investigation (equal); Writing – original draft (equal). **Adnan Munir:** Conceptualization (equal); Project administration (equal); Supervision (equal); Writing – original draft (equal). **Ming Zhao:** Supervision (equal); Writing – review & editing (equal). **Umar Farooq:** Data curation (equal); Investigation (equal); Writing – review & editing (equal). **M. Nafees Mumtaz Qadri:** Formal analysis (equal); Investigation (equal); Writing – review & editing (equal). **Mohammad S. Islam:** Conceptualization (equal); Project administration (equal); Supervision (equal); Writing – review & editing (equal).

DATA AVAILABILITY

The data that support the findings of this study are available from the corresponding author upon reasonable request.

REFERENCES

[1]S. L. Wright, J. Ulke, A. Font, K. L. A. Chan, and F. J. Kelly, "Atmospheric microplastic deposition in an urban environment and an evaluation of transport," Environ. Int. **136**, 105411 (2020).
[2]X. Lim, "Microplastics are everywhere—But are they harmful," Nature **593**(7857), 22–25 (2021).
[3]Q. Chen *et al.*, "An emerging role of microplastics in the etiology of lung ground glass nodules," Environ. Sci. Eur. **34**(1), 25 (2022).
[4]D. Carrington, *Microplastics Found Deep in Lungs of Living People for First Time* (The Guardian, 2022).
[5]L. C. Jenner, J. M. Rotchell, R. T. Bennett, M. Cowen, V. Tentzeris, and L. R. Sadofsky, "Detection of microplastics in human lung tissue using μFTIR spectroscopy," Sci. Total Environ. **831**, 154907 (2022).
[6]L. F. Amato-Lourenço, R. Carvalho-Oliveira, G. R. Júnior, L. dos Santos Galvão, R. A. Ando, and T. Mauad, "Presence of airborne microplastics in human lung tissue," J. Hazard. Mater. **416**, 126124 (2021).
[7]S. Huang *et al.*, "Detection and analysis of microplastics in human sputum," Environ. Sci. Technol. **56**(4), 2476–2486 (2022).
[8]J. C. Prata, "Microplastics and human health: Integrating pharmacokinetics," Crit. Rev. Environ. Sci. Technol. **53**(16), 1489–1511 (2023).
[9]Z. Yang *et al.*, "Human microplastics exposure and potential health risks to target organs by different routes: A review," Curr. Pollut. Rep. **9**(3), 468–485 (2023).
[10]A. Al Mamun, T. A. E. Prasetya, I. R. Dewi, and M. Ahmad, "Microplastics in human food chains: Food becoming a threat to health safety," Sci. Total Environ. **858**, 159834 (2023).
[11]M. Jin, X. Wang, T. Ren, J. Wang, and J. Shan, "Microplastics contamination in food and beverages: Direct exposure to humans," J. Food Sci. **86**(7), 2816–2837 (2021).
[12]G. E. De-la-Torre, "Microplastics: An emerging threat to food security and human health," J. Food Sci. Technol. **57**(5), 1601–1608 (2020).
[13]L. F. Amato-Lourenço, L. dos Santos Galvão, L. A. de Weger, P. S. Hiemstra, M. G. Vijver, and T. Mauad, "An emerging class of air pollutants: Potential effects of microplastics to respiratory human health?," Sci. Total Environ. **749**, 141676 (2020).
[14]K. Perera, S. Ziajahromi, S. B. Nash, and F. D. L. Leusch, "Microplastics in Australian indoor air: Abundance, characteristics, and implications for human exposure," Sci. Total Environ. **889**, 164292 (2023).
[15]F. Huang *et al.*, "Role of CFD based *in silico* modelling in establishing an *in vitro-in vivo* correlation of aerosol deposition in the respiratory tract," Adv. Drug Delivery Rev. **170**, 369–385 (2021).
[16]U. Farooq, H. H. Riaz, A. Munir, M. Zhao, A. Tariq, and M. S. Islam, "Application of heliox for optimized drug delivery through respiratory tract," Phys. Fluids **35**(10), 103321 (2023).
[17]M. M. Rahman, M. Zhao, M. S. Islam, K. Dong, and S. C. Saha, "A numerical study on sedimentation effect of dust, smoke and traffic particle deposition in a realistic human lung," Int. J. Multiphase Flow **171**, 104685 (2024).
[18]M. S. Islam *et al.*, "How SARS-CoV-2 Omicron droplets transport and deposit in realistic extrathoracic airways," Phys. Fluids **34**(11), 113320 (2022).
[19]M. S. Islam *et al.*, "How severe acute respiratory syndrome coronavirus-2 aerosol propagates through the age-specific upper airways," Phys. Fluids **33**(8), 081911 (2021).

[20]E. R. Weibel, "Geometric and dimensional airway models of conductive, transitory and respiratory zones of the human lung," Morphom. Human Lung 136–142 (1963).
[21]K. Horsfield and G. Cumming, "Angles of branching and diameters of branches in the human bronchial tree," Bull. Math. Biophys. **29**, 245–259 (1967).
[22]H. Mortazavi, H. M. Beni, M. S. Islam, and G. Paul, "Aerosolized airborne bacteria and viruses inhalation: Micro-bioaerosols deposition effects through upper nasal airway inhalation," in *Digital Human Modeling and Medicine* (Elsevier, 2023), pp. 275–288.
[23]Y. Yan, J. Dong, and J. Tu, "Comparative modelling of inspiratory airflow and micron particle deposition patterns in monkey and human nasal airways," J. Aerosol Sci. **167**, 106099 (2023).
[24]A. Haghnegahdar, R. Bharadwaj, and Y. Feng, "Exploring the role of nasal hair in inhaled airflow and coarse dust particle dynamics in a nasal cavity: A CFD-DEM study," Powder Technol. **427**, 118710 (2023).
[25]P. Larpruenrudee *et al.*, "Ultrafine particle transport to the lower airways: Airway diameter reduction effects," in *Digital Human Modeling and Medicine* (Elsevier, 2023), pp. 253–274.
[26]M. S. Islam *et al.*, "Polydisperse aerosol transport and deposition in upper airways of age-specific lung," Int. J. Environ. Res. Public Health **18**(12), 6239 (2021).
[27]M. Biglarian, M. MomeniLarimi, B. Firoozabadi, K. Inthavong, and A. Farnoud, "Targeted drug delivery with polydisperse particle transport and deposition in patient-specific upper airway during inhalation and exhalation," Respir. Physiol. Neurobiol. **308**, 103986 (2023).
[28]Y. Cheng, H. Yu, S. Xie, J. Zhao, and Y. Ye, "Study on the coal dust deposition fraction and site in the upper respiratory tract under different particle sizes and labor intensities," Sci. Total Environ. **868**, 161617 (2023).
[29]K. Kadota *et al.*, "*In silico* evaluation of particle transport and deposition in the airways of individual patients with chronic obstructive pulmonary disease," Eur. J. Pharm. Biopharm. **174**, 10–19 (2022).
[30]M. M. Rahman, M. Zhao, M. S. Islam, K. Dong, and S. C. Saha, "Numerical study of nanoscale and microscale particle transport in realistic lung models with and without stenosis," Int. J. Multiphase Flow **145**, 103842 (2021).
[31]M. Malvè, C. Sánchez-Matás, and J. L. López-Villalobos, "Modelling particle transport and deposition in the human healthy and stented tracheobronchial airways," Ann. Biomed. Eng. **48**, 1805–1820 (2020).
[32]P. K. Rajaraman *et al.*, "Transport and deposition of hygroscopic particles in asthmatic subjects with and without airway narrowing," J. Aerosol Sci. **146**, 105581 (2020).
[33]P. K. Rajaraman, J. Choi, A. Babiskin, R. Walenga, and C.-L. Lin, "Transport and deposition of beclomethasone dipropionate drug aerosols with varying ethanol concentration in severe asthmatic subjects," Int. J. Pharm. **636**, 122805 (2023).
[34]M. S. Islam *et al.*, "How microplastics are transported and deposited in realistic upper airways?," Phys. Fluids **35**(6), 063319 (2023).
[35]A. Arsalanloo, M. Abbasalizadeh, M. Khalilian, Y. Saniee, A. Ramezanpour, and M. S. Islam, "A computational approach to understand the breathing dynamics and pharmaceutical aerosol transport in a realistic airways," Adv. Powder Technol. **33**(7), 103635 (2022).
[36]D. Ciloglu, "A numerical study of the aerosol behavior in intra-acinar region of a human lung," Phys. Fluids **32**(10), 103305 (2020).
[37]H. Jing *et al.*, "Large eddy simulation study of the airflow characteristics in a human whole-lung airway model," Phys. Fluids **35**(7), 071903 (2023).
[38]H. Jing *et al.*, "Investigating unsteady airflow characteristics in the human upper airway based on the clinical inspiration data," Phys. Fluids **35**(10), 101911 (2023).
[39]A. Haider and O. Levenspiel, "Drag coefficient and terminal velocity of spherical and nonspherical particles," Powder Technol. **58**(1), 63–70 (1989).
[40]H. Wadell, "The coefficient of resistance as a function of Reynolds number for solids of various shapes," J. Franklin Inst. **217**(4), 459–490 (1934).
[41]J. Xi and P. W. Longest, "Effects of oral airway geometry characteristics on the diffusional deposition of inhaled nanoparticles," J. Biomech. Eng. **130**(1), 011008 (2008).
[42]K.-H. Cheng and D. L. Swift, "Calculation of total deposition fraction of ultrafine aerosols in human extrathoracic and intrathoracic regions," Aerosol Sci. Technol. **22**(2), 194–201 (1995).
[43]P. W. Longest and J. Xi, "Effectiveness of direct Lagrangian tracking models for simulating nanoparticle deposition in the upper airways," Aerosol Sci. Technol. **41**(4), 380–397 (2007).
[44]S. M. Bowes III and D. L. Swift, "Deposition of inhaled particles in the oral airway during oronasal breathing," Aerosol Sci. Technol. **11**(2), 157–167 (1989).
[45]T. L. Chan and M. Lippmann, "Experimental measurements and empirical modelling of the regional deposition of inhaled particles in humans," Am. Ind. Hyg. Assoc. J. **41**(6), 399–409 (1980).
[46]Y.-S. Cheng, Y. Zhou, and B. T. Chen, "Particle deposition in a cast of human oral airways," Aerosol Sci. Technol. **31**(4), 286–300 (1999).
[47]P. C. Emmett, R. J. Aitken, and W. J. Hannan, "Measurements of the total and regional deposition of inhaled particles in the human respiratory tract," J. Aerosol Sci. **13**(6), 549–560 (1982).
[48]N. Foord, A. Black, and M. Walsh, "Regional deposition of 2.5–7.5 μm diameter inhaled particles in healthy male non-smokers," J. Aerosol Sci. **9**(4), 343–357 (1978).
[49]C. Kleinstreuer, Z. Zhang, Z. Li, W. L. Roberts, and C. Rojas, "A new methodology for targeting drug-aerosols in the human respiratory system," Int. J. Heat Mass Transfer **51**(23–24), 5578–5589 (2008).
[50]M. Lippmann and R. E. Albert, "The effect of particle size on the regional deposition of inhaled aerosols in the human respiratory tract," Am. Ind. Hyg. Assoc. J. **30**(3), 257–275 (1969).
[51]W. Stahlhofen, J. Gebhart, and J. Heyder, "Experimental determination of the regional deposition of aerosol particles in the human respiratory tract," Am. Ind. Hyg. Assoc. J. **41**(6), 385–398a (1980).
[52]W. Stahlhofen, J. Gebhart, J. Heyder, and G. Scheuch, "New regional deposition data of the human respiratory tract," J. Aerosol Sci. **14**(3), 186–188 (1983).